

Ni/Al₂O₃ catalysts: effects of the promoters Ce, La and Zr on the methane steam and oxidative reforming reactions

Cite this: *Catal. Sci. Technol.*, 2013, **3**, 635

Tatiana de Freitas Silva,^{*a} Joelmir Augusto Costa Dias,^b
Cristhiane Guimarães Maciel^a and José Mansur Assaf^a

The influence of the promoters CeO₂, CeO₂-ZrO₂ and CeO₂-La₂O₃ on the reactivity of γ -Al₂O₃ supported nickel catalysts from steam and oxidative reforming of methane was investigated in this study. At temperatures above 500 °C, promoted catalysts showed the best performance in the methane oxidative reforming reaction. The increase in activity can be attributed to the specific catalyst-promoter interactions such as the capacity of CeO₂ to store and release oxygen and the influence of La₂O₃ on the stability of the support. Below 500 °C, the activity of the catalyst may be related more directly to the exposed metal surface area.

Received 16th August 2012,
Accepted 11th October 2012

DOI: 10.1039/c2cy20573d

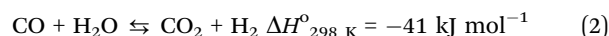
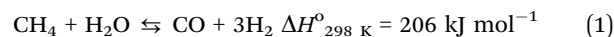
www.rsc.org/catalysis

Introduction

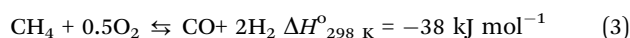
Finite stocks of fossil fuels and pollution problems related to their combustion have led the scientific and industrial communities and governments to search for alternative energy systems.¹ Hydrogen has attracted great interest as a future clean fuel to be used in combustion engines and fuel cells.² It can be produced from various sources, like fossil fuels and sustainable sources.³ The electrolytic production of hydrogen by electric power from solar cells or from hydroelectricity is considered the cleanest and most desirable method, but nowadays these processes do not provide enough hydrogen.⁴

The conversion of petroleum or natural gas products into hydrogen has generally been achieved by one of the following processes: steam reforming (SR), partial oxidation (PO), autothermal reforming (ATR), dry reforming (DR) or a combination of two or more of these processes.⁵ Steam reforming is the principal industrial catalytic process for the conversion of methane into synthesis gas (syngas) to be used in H₂ generation,² as shown in eqn (1). The H₂ : CO ratio produced in reaction (1) is 3 : 1, making this process suitable for hydrogen

production. The water-gas shift reaction takes place in parallel with reaction (1) and is represented by eqn (2).



The stoichiometry of eqn (1) suggests that one mol of H₂O is needed to convert one mol of methane; however, excess steam must be used, in order to avoid the formation of carbon deposits on the catalyst. The ratio H₂O : CH₄ = 2.5–3.0 : 1 is used in industrial plants that operate with natural gas.^{2,6} Even though this is the route employed most frequently in the industry, it has the disadvantage of high energy costs, since it is an endothermic reaction,⁷ making the high temperatures necessary to provide high levels of methane conversion. Besides this, the necessity of operating under such severe conditions leads to catalyst deactivation by sintering or by coke formation, since the catalyst starts the promotion of parallel reactions that form carbon on the catalyst surface.⁷ An alternative process, which could decrease the energy costs of hydrogen production, is the partial oxidation of methane (POM).⁸ In this process, methane is oxidized to produce CO and H₂:



The most important characteristic of POM applied to the production of H₂ or synthesis gas is that the reaction is moderately exothermic. On the other hand, methane steam reforming produces a higher H₂/CO ratio than partial oxidation, favoring the hydrogen production.^{9,10}

^a Laboratório de Catálise – Departamento de Engenharia Química, Universidade Federal de São Carlos, Via Washington Luiz, Km 235, CEP: 13565-905, São Carlos, SP, Brazil. E-mail: tatianaufv@yahoo.com.br; Fax: +55 16 3351 8266; Tel: +55 16 8807 2585

^b PETROBRAS-REPLAN – Refinaria de Paulínia – Via SP-332, km 132, CEP 13140-000 Paulínia, SP, Brazil

One way to minimize energetic costs in hydrogen production is to combine steam reforming of methane (SRM) and POM. This is done by performing methane steam reforming in the presence of oxygen.⁴ This set of reactions requires less energy than SRM, given the exothermic contribution of partial oxidation, and it may improve the temperature control in the reactor and reduce the formation of hot spots, thus avoiding catalyst deactivation by sintering or carbon deposition.⁴ Its main advantage is that the heat generated by methane partial oxidation can be used as a source of energy in the endothermic reactions. Various studies have been focused on Ni/Al₂O₃ catalysts, to which promoters are added in order to improve support stability and carbon removal, increase metal dispersion, *etc.* This paper reports a study of influence of the promoters CeO₂, CeO₂-ZrO₂ and CeO₂-La₂O₃ on the catalytic and surface properties of Ni/Al₂O₃.

Experimental

Preparation of supports and catalysts

The catalysts were prepared by wet impregnation. Particles of γ -Al₂O₃ (Alfa Aesar) were selected on a 100–200 mesh and calcined at 550 °C for 5 hours in synthetic air flowing at 80 mL min⁻¹ in order to remove volatile compounds. Precursor salts used to obtain oxides of cerium, cerium-zirconium and cerium-lanthanum were Ce(NO₃)₃·6H₂O (Fluka), Cl₂OZr·8H₂O (Fluka) and La(NO₃)₃·xH₂O (Aldrich) respectively. The final content of promoter (w/w) was 10% of the alumina support. It is important to emphasize that when two precursors were used on alumina, only one solution was prepared, allowing the oxides to be randomly deposited on alumina. The samples were again calcined under the same conditions used for γ -alumina. The active phase was also added to the supports by wet impregnation, with an amount of Ni(NO₃)₂·6H₂O (Aldrich) sufficient to yield 15% nickel by weight. The calcined supports were impregnated with this solution in a rotary evaporator with constant stirring at 70 °C until the sample was homogeneous. After nickel oxide impregnation, the catalysts were dried for 24 hours and then calcined (under the same conditions as the other precursors).

Catalyst characterization

The physicochemical properties of the catalysts were measured by energy-dispersive X-ray spectroscopy (EDS), BET analysis of surface area, X-ray diffraction (XRD), temperature-programmed reduction (H₂-TPR), temperature-programmed hydrogen desorption (H₂-TPD) and temperature-programmed oxidation (TPO). The EDS analysis was performed in an Oxford 7060 energy-dispersive analyzer based on Si (Li) with a beryllium window and a resolution of 133 eV. The specific areas of the catalysts were determined in a Quantachrome NOVA 1200; for the BET analysis, about 200 mg of sample was previously activated at 300 °C in nitrogen and then cooled to -195 °C, to allow the physical adsorption of N₂. H₂-TPR measurements were performed in a Micromeritics Pulse ChemSorb 2705 equipped with a thermal conductivity detector (TCD), using 30 mg of sample.

The X-ray diffraction patterns were collected with a Rigaku Multiflex diffractometer, the Bragg angle being varied from 10° to 80° at 2° min⁻¹, using Cu K α radiation with a nickel filter. Both the NiO and CeO₂ apparent crystallite sizes (D_{NiO} and D_{CeO_2} , respectively) were determined by Scherrer's equation, using the reflection (2 0 0) for NiO and the reflection (1 1 1) for CeO₂. In order to calculate the metal surface area of the catalyst, H₂-TPD analysis was performed in the same equipment as the H₂-TPR measurements. 100 mg of catalyst was reduced for 2 hours at 700 °C in pure H₂. Next, the sample was cooled to 25 °C in N₂ flowing at 30 mL min⁻¹. At this temperature, the sample was subjected to a 30 mL min⁻¹ flow of pure hydrogen for 1 hour until saturated with adsorbed H₂. The hydrogen was then purged by N₂ flowing at 30 mL min⁻¹ for 2 hours to expel accumulated hydrogen from the pores, so that only chemisorbed hydrogen would remain in the catalyst. After the purging process, the hydrogen desorption measurement started in a 30 mL min⁻¹ flow of nitrogen, with a heating rate of 10 °C min⁻¹ up to 700 °C, and the sample remained at that temperature until the end of the measurement. TPO analyses were performed on the catalyst samples after they were used in the catalytic tests, in a TA Instruments SDT2960 simultaneous DSC-TGA instrument; samples were heated to 900 °C at 10 °C min⁻¹ in an oxidizing atmosphere (synthetic air).

Catalytic experiments

Methane oxidative reforming experiments were performed in a quartz reactor of internal diameter 0.9 cm, with 0.1500 g catalyst samples held between quartz wool plugs. The feed rates were 20 mL min⁻¹ of methane, 47 mL min⁻¹ of air (21.3% O₂) and 3.9 g h⁻¹ of water at 25 °C and 1 atm. The CH₄ : H₂O : O₂ molar ratio in the feed was thus 1 : 4 : 0.5. In steam reforming experiments, the same amount of sample and the same conditions of pressure and temperature were used. The SRM feed rates were 40 mL min⁻¹ of methane and 7.10 g h⁻¹ of water, giving a CH₄ : H₂O molar ratio of 1 : 4. All catalysts were initially reduced with pure H₂ flowing at 30 mL min⁻¹, the sample being heated at 10 °C min⁻¹ to 700 °C, where it remained for three hours.

Catalytic tests were performed at temperatures falling from 700 °C to 350 °C in steps of 50 °C. Gas chromatography (GC) was performed on the outlet gases in triplicate at each temperature step, after a few minutes had elapsed, in order to allow the reaction system to stabilize. These GC analyses were performed by a VARIAN 3800 chromatograph equipped with thermal conductivity detectors (TCDs). Effluents were split into two streams. The first stream had helium as the carrier gas, flowing with 25 mL min⁻¹, the analytes being separated on a 13X column in series with a PORAPAK column. The second stream had nitrogen as the carrier gas, flowing at 25 mL min⁻¹, separated on a molecular sieve 13X column. Both streams were monitored with TCDs. The feed gas flow rate was controlled by a mass flow controller (MKS Instruments 247, with 4 channels). Liquid water was fed through a high-pressure piston pump with a flow rate digital control.

Results and discussion

A semi-quantitative estimate of the percentage of metal elements present in each catalyst was obtained by EDS analysis. The results (Table 1) are an average of 3 measurements of the mass fraction. The results showed differences in nominal and real composition. This may be caused by a heterogeneous distribution of the components in the catalytic matrix added by the accuracy of the EDS analysis, causing the material in the bulk of the catalyst to be not fully detected.

The surface areas of the catalyst samples measured by the BET method are shown in Table 1. Alumina has the highest surface area and the metal oxides addition causes a decrease in the surface area. The elevated values showed by the catalysts are due to alumina characteristics, which present an area of $196 \text{ m}^2 \text{ g}^{-1}$. Also, it is possible to note that the presence of promoters decreases the specific area, probably due to coating of alumina pores. Cerium addition causes an accentuated decrease in $\text{NiO}/\gamma\text{-Al}_2\text{O}_3$, but the BET area with addition of zirconium in $\text{NiO}/\text{CeO}_2\text{-Al}_2\text{O}_3$ had a similar value. Also, the lanthanum addition in $\text{NiO}/\text{CeO}_2\text{-Al}_2\text{O}_3$ causes an accentuated decrease, probably due to La_2O_3 coverage of alumina pores.

The X-ray diffraction patterns for all the samples are shown in Fig. 1. All catalysts produced diffraction peaks of low intensity, characteristic of $\gamma\text{-Al}_2\text{O}_3$, indicating low support crystallinity.¹¹ The $\text{NiO}/\text{CeO}_2\text{-Al}_2\text{O}_3$ sample showed peaks related to CeO_2 at 28.7° , 33.1° , 47.7° , 56.6° , 59.6° and 77.0° , the peak at 28.7° having the greatest intensity. These peaks were generated by the face-centered cubic (fcc) structure of fluorite-type cerium oxide.^{12–15} CeO_2 -related peaks of the fluorite type were also produced by the $\text{NiO}/\text{CeO}_2\text{-ZrO}_2\text{-Al}_2\text{O}_3$ and $\text{NiO}/\text{CeO}_2\text{-La}_2\text{O}_3\text{-Al}_2\text{O}_3$ samples. The addition of Zr on the cerium oxide crystal lattice should cause a shift of these peaks to higher values of 2θ .¹⁶ Such a change in the position of these peaks is usually cited as evidence that Zr has entered the cerium oxide crystal lattice, giving rise to a solid solution with a cubic structure with a reduced cerium oxide lattice parameter. In this study, there were no significant peak changes; thus, there is no evidence that zirconium entered the cerium oxide crystal lattice. The absence of any diffraction peaks for the ZrO_2 phase may be due to small and dispersed particles.¹⁷

The $\text{NiO}/\text{CeO}_2\text{-La}_2\text{O}_3\text{-Al}_2\text{O}_3$ sample did not show any peaks related to La_2O_3 , to non-stoichiometric species (LaO_x) or to lanthanum aluminate. According to the EDS result shown in Table 1, the absence of those peaks may be due to the lanthanum content being undetectable by X-ray diffraction.¹⁸

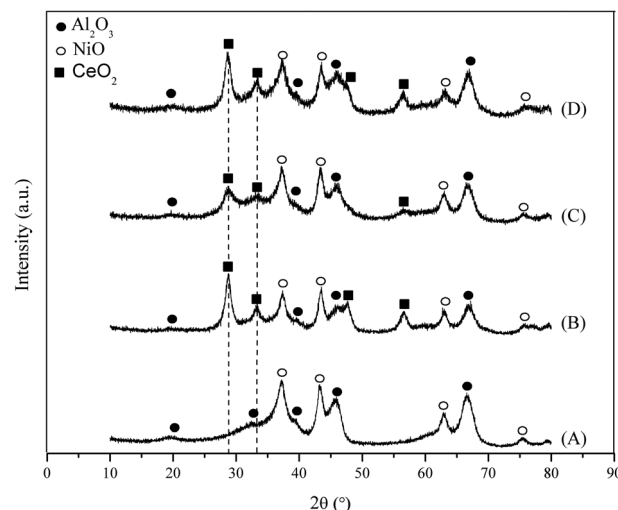


Fig. 1 XRD patterns of catalysts. (A) $\text{NiO}/\text{Al}_2\text{O}_3$; (B) $\text{NiO}/\text{CeO}_2\text{-Al}_2\text{O}_3$; (C) $\text{NiO}/\text{CeO}_2\text{-ZrO}_2\text{-Al}_2\text{O}_3$; (D) $\text{NiO}/\text{CeO}_2\text{-La}_2\text{O}_3\text{-Al}_2\text{O}_3$.

NiO and CeO_2 crystallite sizes of all samples were estimated from Scherrer's equation and the results are presented in Table 1. These results show that NiO is present as small particles in the range of 5–7 nm in all catalysts, the $\text{NiO}/\text{CeO}_2\text{-Al}_2\text{O}_3$ being the one which presented the biggest crystallite sizes. For the catalysts promoted with ceria, the $\text{NiO}/\text{CeO}_2\text{-ZrO}_2\text{-Al}_2\text{O}_3$ catalyst showed the smallest crystallite size related to CeO_2 (4.1 nm). The addition of ZrO_2 to CeO_2 caused a decrease in the crystallite size. According to the literature, the use of ZrO_2 improves the thermal stability of CeO_2 , avoiding the sintering process.^{19,20}

The H_2 -TPR reduction profiles of $\text{NiO}/\gamma\text{-Al}_2\text{O}_3$, $\text{NiO}/\text{CeO}_2\text{-Al}_2\text{O}_3$, $\text{NiO}/\text{CeO}_2\text{-ZrO}_2\text{-Al}_2\text{O}_3$ and $\text{NiO}/\text{CeO}_2\text{-La}_2\text{O}_3\text{-Al}_2\text{O}_3$ samples are shown in Fig. 2. By comparing these results with data in the literature, the peaks at low reduction temperatures (approximately at 227°C to 420°C) can be attributed to the reduction of free nickel oxides that interact weakly with the support. Such peaks can be seen in the profiles for $\text{NiO}/\gamma\text{-Al}_2\text{O}_3$ and $\text{NiO}/\text{CeO}_2\text{-Al}_2\text{O}_3$. A small shoulder may represent reduction of this species in $\text{NiO}/\text{CeO}_2\text{-ZrO}_2\text{-Al}_2\text{O}_3$ and $\text{NiO}/\text{CeO}_2\text{-La}_2\text{O}_3\text{-Al}_2\text{O}_3$. All the catalysts, except $\text{NiO}/\text{CeO}_2\text{-Al}_2\text{O}_3$, show the largest reduction peak for NiO species around 600°C , implying that these species interact moderately with the support. In the $\text{NiO}/\text{CeO}_2\text{-Al}_2\text{O}_3$ catalyst, that peak is shifted to about 570°C , indicating that these species are reduced more readily than in other catalysts. The reduction peaks above 800°C correspond to

Table 1 Average elemental composition of catalysts obtained by EDS, specific surface area of catalysts estimated by the BET method and apparent crystallite size (D_{NiO} and D_{CeO_2})

Catalysts	Ni (wt%)	Ce (wt%)	Zr (wt%)	La (wt%)	BET surface area/ $\text{m}^2 \text{ g}_{\text{cat}}^{-1}$	D_{NiO}/nm	$D_{\text{CeO}_2}/\text{nm}$
$\text{NiO}/\gamma\text{-Al}_2\text{O}_3$	17.89	—	—	—	195.9	5.3	—
$\text{NiO}/\text{CeO}_2\text{-Al}_2\text{O}_3$	17.07	8.04	—	—	136.0	6.6	7.6
$\text{NiO}/\text{CeO}_2\text{-ZrO}_2\text{-Al}_2\text{O}_3$	13.81	4.65	7.55	—	129.8	5.1	4.1
$\text{NiO}/\text{CeO}_2\text{-La}_2\text{O}_3\text{-Al}_2\text{O}_3$	16.92	4.25	—	3.24	103.7	4.6	6.2

g_{cat} = gram of catalyst.

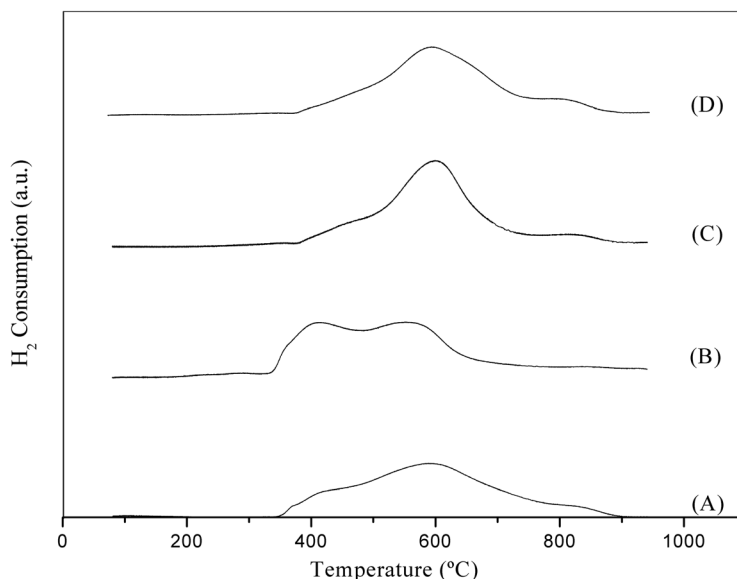


Fig. 2 H_2 -TPR profiles of catalysts. (A) $NiO/\gamma-Al_2O_3$, (B) $NiO/CeO_2-Al_2O_3$, (C) $NiO/CeO_2-ZrO_2-Al_2O_3$ and (D) $NiO/CeO_2-La_2O_3-Al_2O_3$.

the formation of nickel aluminate, evidently in strong interaction with the support. It is interesting to observe that the $NiO/CeO_2-Al_2O_3$ catalyst has a large fraction of Ni^{2+} that interacts more weakly, producing a peak at 327 to 527 °C.²¹

In the H_2 -TPR studies, a CuO standard was used to calibrate the degree reduction of Ni^{2+} . The amount of reduced Ni^{2+} was calculated by integrating the reduction peaks in the H_2 -TPR profiles and expressed as a percentage of the consumption needed to reduce all the Ni^{2+} in the catalysts, based on the elemental contents of Ni determined by EDS. Since reduction of ceria also occurs, values of H_2 consumption by the Ni catalysts containing Ce were adjusted by subtracting the consumption of the $CeO_2-Al_2O_3$ support. This support was subjected to H_2 -TPR and generated peaks at 400–600 °C related to the reduction of ceria on the surface, and at 800–900 °C, related to reduction of bulk ceria (Fig. 6). Table 2 presents the percent reduction of Ni^{2+} calculated for the four catalysts. The $NiO/CeO_2-ZrO_2-Al_2O_3$ catalyst presented the highest reduction (100%), indicating that all the Ni was reduced to Ni^0 , while the percent reduction of Ni in the catalysts $NiO/CeO_2-Al_2O_3$ and $NiO/CeO_2-La_2O_3-Al_2O_3$ was slightly smaller than in the non-promoted catalyst. The higher hydrogen consumption observed for the sample $Ni/CeO_2-ZrO_2-Al_2O_3$ compared to $NiO/CeO_2-Al_2O_3$ is attributed to the addition of zirconium in the crystalline lattice of ceria, which helps its reducibility. Zirconium oxide promotes the formation of vacancies

in the cerium oxide's crystal lattice, which facilitate oxygen removal in the catalytic surface, thus increasing the consumption of H_2 .^{20–22}

Fig. 3 shows the H_2 -TPD profiles of the catalysts. Different peaks can be observed in the H_2 -TPD profiles and that there are sites with different adsorption forces. Promoters shift the peaks to higher or lower temperatures, that is, they cause stronger or weaker H_2 chemisorption. These shifts may be attributed to electronic changes due to the formation of alloys, since hydrogen adsorption and desorption are not sensitive to particle size.²³ The desorption profile of the $NiO/CeO_2-ZrO_2-Al_2O_3$ catalyst is different from other catalysts. These differences can be attributed to the influence of zirconium on the interaction of hydrogen with the nickel surface.¹⁸ The catalyst $NiO/CeO_2-Al_2O_3$ presented a peak shift to higher temperatures, indicating stronger sites relative to the other ones. Also it has the largest area under the peaks, indicating a highest amount of adsorbed sites.

Table 3 shows the metal surface area and percent dispersion of the catalysts not containing Zr . According to the literature,²⁴ it is not correct to estimate the metal area of catalysts containing Zr by this technique, as the amounts of H_2 chemisorbed on the surface of zirconia are readily dissolved in it as the temperature rises.

The $NiO/CeO_2-La_2O_3-Al_2O_3$ catalyst has a smaller metal surface area than $NiO/\gamma-Al_2O_3$. This decrease might be due to the aggregation of nickel into larger particles after reduction, facilitated by ceria-lanthanum-alumina interaction with the metallic sites. The $NiO/CeO_2-Al_2O_3$ catalyst showed the largest specific metal area, and the ceria-alumina interaction favors the nickel smaller crystals growth. Addition of lanthanum in the $NiO/CeO_2-Al_2O_3$ catalyst causes a decrease in the dispersion. This behavior was also noted by Navarro *et al.*¹⁵ and Araujo *et al.*,²⁵ who observed decreases in values of Pt dispersion with the addition of La_2O_3 to the supports of Al_2O_3 . According to the authors, this decrease is attributed to the coating of metallic

Table 2 Hydrogen consumed by the catalysts during TPR

Catalysts	Theoretical H_2 consumption (10^{-5} mol)	Actual H_2 consumed (10^{-5} mol)	Degree of reduction (%)
$NiO/\gamma-Al_2O_3$	9.14	7.85	86
$NiO/CeO_2-Al_2O_3$	8.72	6.75	77
$NiO/CeO_2-ZrO_2-Al_2O_3$	7.06	7.04	100
$NiO/CeO_2-La_2O_3-Al_2O_3$	8.65	6.71	78

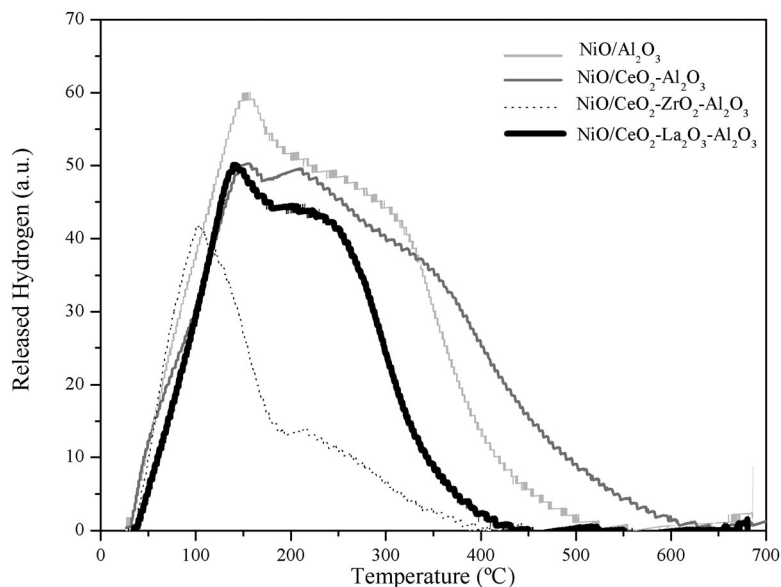


Fig. 3 H₂-TPD profiles of catalysts.

Table 3 Metal surface area and dispersion estimated by TPD

Catalysts	Metallic area/m ² g _{cat} ⁻¹	Dispersion (%)
NiO/γ-Al ₂ O ₃	13.8	2.8
NiO/CeO ₂ -Al ₂ O ₃	15.1	2.6
NiO/CeO ₂ -La ₂ O ₃ -Al ₂ O ₃	10.2	2.1

particles by lanthanum oxide. Thus, in the present work, the decrease in metal dispersion displayed for the sample promoted with CeO₂ and La₂O₃ could be associated to the covering of the support by Ni.

Fig. 4 shows the total methane conversion results in the methane oxidative reforming tests. It can be seen that above 500 °C, the unpromoted catalyst produced the lowest total conversion and higher rates of conversion are achieved with the promoters. It has been reported that the addition of ZrO₂ to

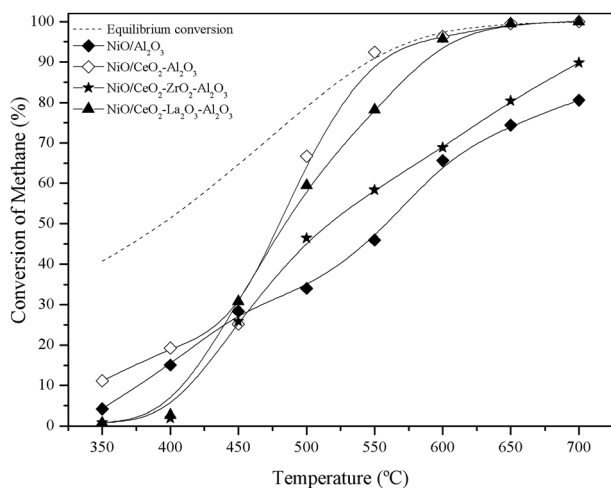


Fig. 4 Methane conversion during oxidative reforming.

CeO₂ leads to improvement in its oxygen storage capacity, redox properties, thermal resistance and catalytic activity at low temperatures.²⁶ Cerium and cerium-zirconium oxides have important roles in maintaining the catalytic bed free of carbon, due to their redox properties. La₂O₃ also has the property of removing carbon from the catalyst surface, and stabilizing the support.

The NiO/CeO₂-Al₂O₃ catalyst showed the greatest catalytic activity below 500 °C. At low temperatures there is a sharp fall in conversion. This may be due to the oxidation of metallic nickel. Above 500 °C, methane conversion increase greatly with rising temperature, especially on the NiO/CeO₂-Al₂O₃ and NiO/CeO₂-La₂O₃-Al₂O₃ catalysts, and, above 600 °C, the conversion on those catalysts reaches the equilibrium conversion (almost 100%).

Fig. 5 presents the effluent composition for nickel catalysts supported by Al₂O₃, CeO₂-Al₂O₃, CeO₂-La₂O₃-Al₂O₃ and CeO₂-ZrO₂-Al₂O₃ for the oxidative reforming reaction. By analyzing Fig. 5, it can be observed that H₂ production is favorable at high temperatures for all catalysts. Below 500 °C, there is discrete H₂ production, and above 500 °C the H₂ molar fraction increases drastically. It can be noted that the mole fraction of carbon dioxide is higher than that of carbon monoxide. The largest amount of carbon dioxide is due to the excess of water used in the reaction, which favored the shift reaction positively (eqn (2)). It is important to note that above 500 °C the amount of oxygen is practically zero, indicating that the combustion of methane occurs. It is possible to observe that the addition of ceria and zirconia in the NiO/Al₂O₃ catalysts favors the catalytic properties and specially the ratio H₂/CO. For H₂ production applications, the ceria and zirconia addition is favorable in oxidative reforming reactions.

Fig. 6 shows the temperature profile of methane conversion on catalysts during methane steam reforming (SRM). Once again, a large increase in conversion with temperature can be

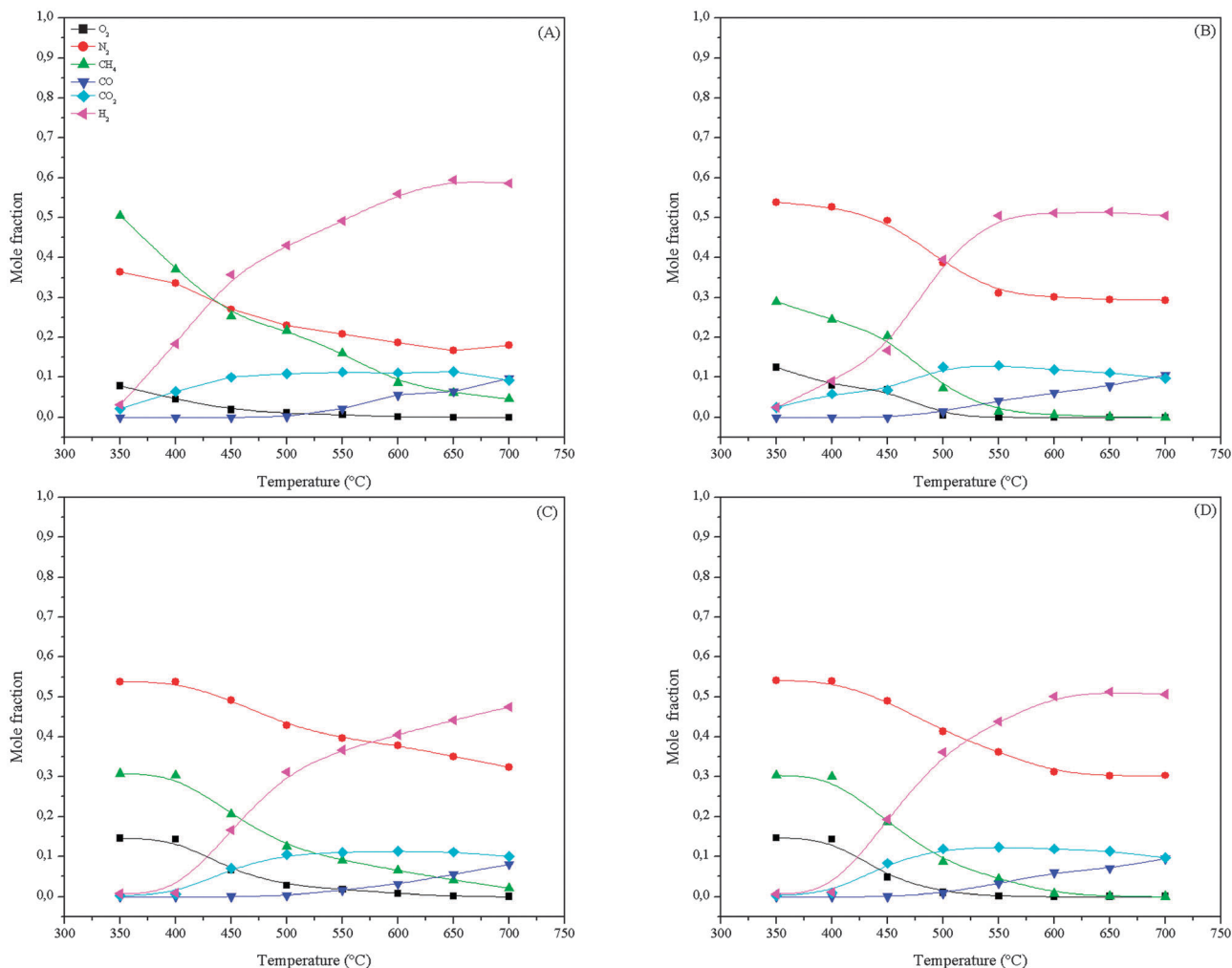


Fig. 5 Mole fraction \times temperature for supported catalysts in oxidative reforming. (A) NiO/Al₂O₃; (B) NiO/CeO₂-Al₂O₃; (C) NiO/CeO₂-ZrO₂-Al₂O₃ and (D) NiO/CeO₂-La₂O₃-Al₂O₃.

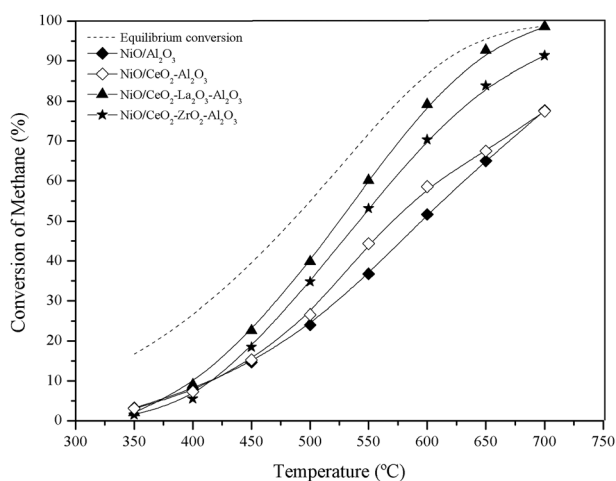


Fig. 6 Methane conversion during steam reforming.

observed; however, the rise is more gradual than in the profile of NiO/CeO₂-Al₂O₃ and NiO/CeO₂-La₂O₃-Al₂O₃ activity during

methane oxidative reforming. It should be noted that the performance of the ZrO₂-promoted catalyst is better in SRM than in oxidative reforming, indicating that Zr is a more effective promoter in steam reforming of methane.

The outlet effluent composition from the catalytic reactor in terms of mole fractions of the steam reforming reaction is illustrated in Fig. 7. In the steam reforming reaction, the methane content decreases whereas the contents of CO, H₂ and CO₂ increase with increasing temperature. It is known that under these conditions, the reactions of steam reforming (eqn (1)) and water-gas shift (eqn (2)) are present in the process. Moreover, carbon dioxide formation is more thermodynamically favored than carbon monoxide's at 350–650 °C because the excess of water in the feed (4 moles of H₂O to 1 mol CH₄) and the interval of temperatures in which the experiments were performed. This is important because it decreases the concentration of carbon monoxide in the product, since this gas causes deactivation by poisoning in the electro-catalyst in low temperature fuel cells (PEM fuel cells). It is also observed that there is a decrease in water intake with increasing temperature,

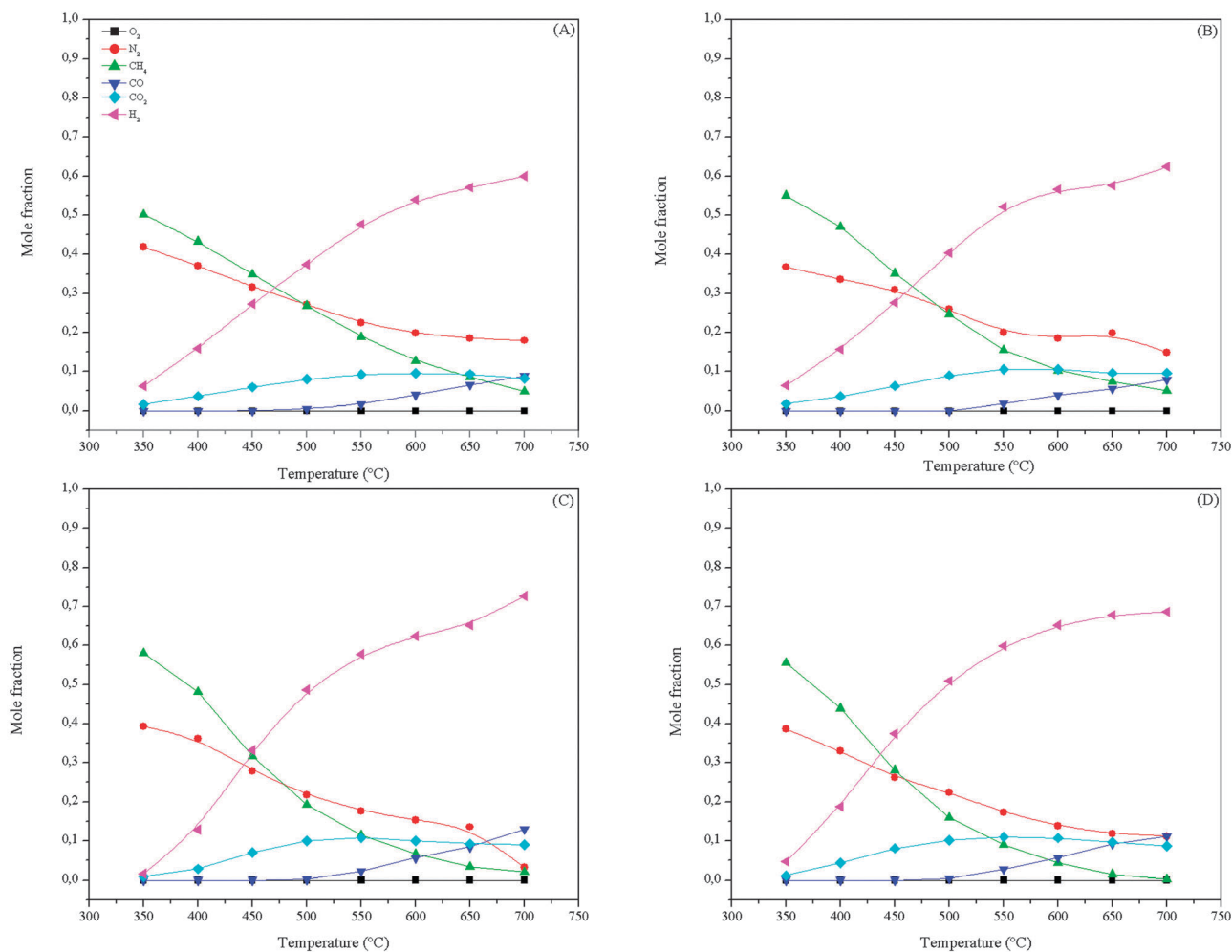


Fig. 7 Mole fraction \times temperature for supported catalysts in steam reforming. (A) NiO/Al_2O_3 ; (B) $NiO/CeO_2-Al_2O_3$; (C) $NiO/CeO_2-ZrO_2-Al_2O_3$ and (D) $NiO/CeO_2-La_2O_3-Al_2O_3$.

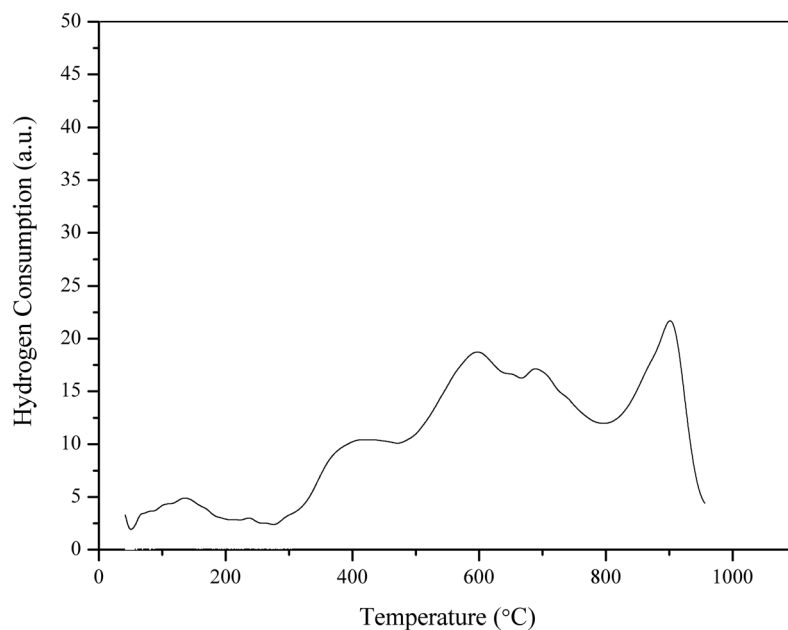


Fig. 8 H_2 -TPR profile of the $CeO_2-Al_2O_3$ support.

Table 4 H₂/CO ratio in products of SR and ATR on supported Ni catalysts

Temperature/°C	NiO/ γ -Al ₂ O ₃		NiO/CeO ₂ -Al ₂ O ₃		NiO/CeO ₂ -ZrO ₂ -Al ₂ O ₃		NiO/CeO ₂ -La ₂ O ₃ -Al ₂ O ₃	
	H ₂ /CO (SR)	H ₂ /CO (ATR)	H ₂ /CO (SR)	H ₂ /CO (ATR)	H ₂ /CO (SR)	H ₂ /CO (ATR)	H ₂ /CO (SR)	H ₂ /CO (ATR)
700	6.8	4.8	7.8	4.8	5.6	6.0	6.1	5.5
650	8.7	6.1	10.2	6.6	7.8	8.1	7.4	7.3
600	13.4	9.2	14.2	8.4	11.1	13.4	11.3	8.5
550	28.7	11.0	29.2	12.6	26.4	24.0	22.5	13.8

as the shift reaction is exothermic. Therefore, the reaction is favored at higher temperatures.

This phenomenon is most visible in Fig. 6, which shows the conversion of methane to carbon monoxide and carbon dioxide. It can be observed that at low temperatures, almost all the carbon monoxide is converted to carbon dioxide, from which the carbon monoxide is only detected at temperatures starting at 500 °C and above, because when the shift reaction approximates to the thermodynamic equilibrium, the conversion tends to fall with increasing temperature, due the reaction being slightly exothermic. This approach to the equilibrium means that, at these temperatures, the rate of increase of conversion with temperature begins to decrease.

By analyzing the H₂-TPR of the Al₂O₃ promoted with Ce (Fig. 8), it can be seen that the reduction of that metal starts at temperatures close to 400 °C, with reduction of surface ceria.

At higher temperatures, bulk ceria, in which the particles are larger, is reduced and the Ce is ready to act as an oxygen storage agent.

This effect is consistent with the sudden increase in the activity of NiO/CeO₂-Al₂O₃ and NiO/CeO₂-La₂O₃-Al₂O₃ catalysts during methane oxidative reforming above 500 °C. However, during steam reforming, since the atmosphere is more reducing, the oxygen storage effect may be ignored, and the metal surface area of the catalyst becomes the reaction limiting factor. This suggestion that the reaction is limited by the metal area would also explain the pattern of methane conversion results at temperatures below 500 °C during methane oxidative reforming.

H₂/CO ratios in the reformed gases are summarized in Table 4. It may be noted that the H₂/CO ratio is lower for the oxidative reforming than steam reforming of methane, at most temperatures and on all catalysts except NiO/CeO₂-ZrO₂-Al₂O₃.

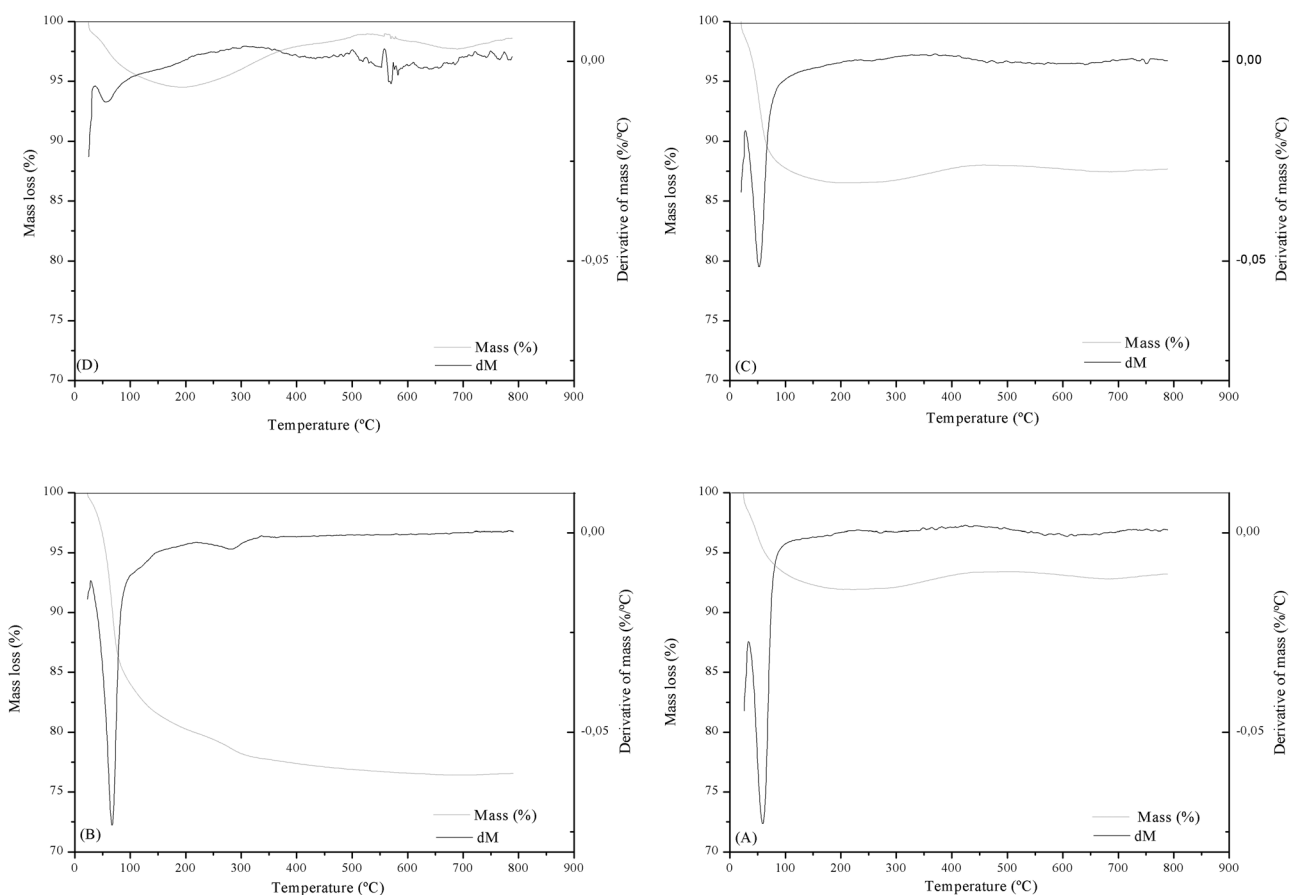
**Fig. 9** Temperature-programmed oxidation profiles. (A) NiO/ γ -Al₂O₃, (B) NiO/CeO₂-Al₂O₃, (C) NiO/CeO₂-ZrO₂-Al₂O₃ and (D) NiO/CeO₂-La₂O₃-Al₂O₃.

Table 5 Carbon deposition on nickel catalysts in the steam reforming determined by thermogravimetry

Catalysts	gC g _{cat} ⁻¹
NiO/γ-Al ₂ O ₃	5.98
NiO/CeO ₂ -Al ₂ O ₃	1.43
NiO/CeO ₂ -ZrO ₂ -Al ₂ O ₃	2.31
NiO/CeO ₂ -La ₂ O ₃ -Al ₂ O ₃	2.37

This shows that H₂ is formed in greater amounts in steam reforming than in the oxidative reforming of methane. It is also important to note that the use of excess of water promotes the WGS reaction, contributing to the formation of carbon dioxide. The reason for the decrease in H₂/CO with increasing temperature is that the shift reaction is less formed at high temperatures.

TPO profiles of the catalysts after the SRM are shown in Fig. 9. Below 200 °C, the mass loss can be ascribed to the liquid retained in the used catalyst, chiefly water. From around 200 to 600 °C, the mass gain reflects the re-oxidation of the metallic Ni still present in the sample. Above 600 °C, the mass losses refer to the removal of coke by gasification. These mass are small and the total mass of C deposited did not exceed 1% in any reaction. The samples presented low carbon content, which can be attributed to excess water in the feed flow, preventing the deposition of carbon. Coke formation results are presented in Table 5. The amount of coke produced decreases in the following order: NiO/Al₂O₃ > NiO/CeO₂-La₂O₃-Al₂O₃ > NiO/CeO₂-ZrO₂-Al₂O₃ > NiO/CeO₂-Al₂O₃ catalysts. Ceria-based catalysts disfavor the carbon deposition, and these results may be related to reducibility and oxygen transfer capacity of CeO₂-Al₂O₃, CeO₂-ZrO₂-Al₂O₃ and CeO₂-La₂O₃-Al₂O₃ systems, hindering the carbon formation by gasification of carbon deposits. The presence of La₂O₃ affects the ability of the catalyst to remove the carbon deposits, probably by activation of H₂O that produces oxygen species that are transferred to carbon. The NiO/CeO₂-Al₂O₃ catalyst presents the lowest carbon deposition compared to the other catalysts, and this fact may be attributed to the elevated amount of ceria.^{25,27–29}

Conclusions

It can be seen that promoted catalysts showed better catalytic activities than the unpromoted ones in the oxidative reforming measurements performed at temperatures higher than 500 °C. The lanthanum oxide may contribute to the stabilization of the support. Zirconia enhances the redox property of ceria, helping to improve the catalytic activity in steam reforming. These effects are more evident at high temperatures, at which cerium oxide goes through an oxidation state change. Below 500 °C, the catalytic activity may be more related to the metal surface area.

Acknowledgements

The authors thank CNPq and FAPESP for their financial support.

References

- 1 D. L. Trimm and Z. I. Önsan, *Catal. Rev.: Sci. Eng.*, 2001, **43**, 31–34.
- 2 J. N. Armor, *Appl. Catal., A*, 1999, **176**, 159–176.
- 3 M. Conte, A. Icobazzi, M. Ronchetti and R. Vellone, *J. Power Sources*, 2001, **100**, 171–181.
- 4 S. Ayabe, H. Omoto, T. Utaka, R. Kikuchi, K. Sasaki, Y. Teraoka and K. Eguchi, *Appl. Catal., A*, 2003, **241**, 261–269.
- 5 P. K. Cheekatamarla and C. M. Finnerty, *J. Power Sources*, 2006, **160**, 490–499.
- 6 H. S. Roh, K. W. Jun, W. S. Dong, J. S. Chang, S. E. Park and Y. Joe, *J. Mol. Catal. A: Chem.*, 2002, **181**, 137–142.
- 7 D. L. Trimm, *J. Catal.*, 1977, **16**, 155–165.
- 8 P. Corbo and F. Migliardini, *Int. J. Hydrogen Energy*, 2007, **32**, 55–66.
- 9 J. A. C. Dias and J. M. Assaf, *J. Power Sources*, 2004, **130**, 106–110.
- 10 M. C. Sánchez, R. M. Navarro and J. L. G. Fierro, *Int. J. Hydrogen Energy*, 2007, **32**, 1462–1471.
- 11 O. V. Mokhnachuk, S. O. Soloviev and A. Y. Kapran, *Catal. Today*, 2007, **119**, 145–151.
- 12 JCPDS - Joint Committee on Powder Diffraction Standards. Int. Center of Diffraction Data (Pennsylvania, USA 2001).
- 13 A. Trovarelli, *Catal. Rev.: Sci. Eng.*, 1996, **38**, 439–520.
- 14 C. Leitenburg, A. Trovarelli, J. Llorca, F. Cavani and G. Bini, *Appl. Catal., A*, 1996, **139**, 161–173.
- 15 R. M. Navarro, M. C. M. C. Alvarez-Galvan, F. Rosa and J. L. G. Fierro, *Appl. Catal., A*, 2006, **297**, 60–72.
- 16 Q. Zhang, M. Shen, J. Wen, J. Wang and Y. Fei, *J. Rare Earths*, 2008, **26**, 347–351.
- 17 N. Srisiriwat, S. Therdthianwong and A. Therdthianwong, *Int. J. Hydrogen Energy*, 2009, **34**, 2224–2234.
- 18 N. R. E. Radwan, *Appl. Catal., A*, 2006, **299**, 103–121.
- 19 J. Kaspar, P. Fornasiero and M. Graziani, *Catal. Today*, 1999, **50**, 285–298.
- 20 X. Zhang, E. Long, Y. Li, J. Guo, L. Zhang, M. Gong, M. Wang and Y. Chen, *J. Nat. Chem.*, 2009, **18**, 139–144.
- 21 L. Znak, K. Stolecki and J. Zielinski, *Catal. Today*, 2005, **101**, 65–71.
- 22 S. C. Dantas, K. A. Resende, R. L. Rossi, A. J. Assis and C. E. Hori, *Chem. Eng. J.*, 2012, **197**, 407–413.
- 23 V. Ponec and G. C. Bond, in *Catalysis by metals and alloys, Studies in Surface Science and Catalysis*, ed. P. Vladimír and C. Geoffrey, Amsterdam/New York, 1995, vol. 95.
- 24 N. Stojilovic, E. T. Bender and R. D. Ramsier, *Prog. Surf. Sci.*, 2005, **78**, 101–184.
- 25 J. C. S. Araujo, D. Zanchet, R. Rinaldi, U. Schuchardt, C. E. Hori, J. L. G. Fierro and J. M. C. Bueno, *Appl. Catal., B*, 2008, **84**, 552–562.
- 26 X. Cai, X. Dong and W. Lin, *J. Nat. Gas Chem.*, 2006, **15**, 122–126.
- 27 X. Karatzas, K. Jansson, A. González, J. Dawody and L. J. Pettersson, *Appl. Catal., B*, 2011, **106**, 476–487.
- 28 Z. Hou, J. Gao, J. Guo, D. Liang, H. Lou and X. Zheng, *J. Catal.*, 2007, **250**, 331–341.
- 29 J. Bussi, N. Bepalko, S. Veiga, A. Amaya, R. Faccio and N. C. Abello, *Catal. Commun.*, 2008, **10**, 33–38.